Analysis of Shear-Dependent Bacterial Adhesion Kinetics to Biomaterial Surfaces

Richard B. Dickinson
Dept. of Chemical Engineering, University of Florida, Gainesville, FL 32611

Stuart L. Cooper
College of Engineering, University of Delaware, Newark, DE 19716

A methodology and analysis is presented to quantitatively characterize bacterial attachment and detachment kinetics on biomaterial surfaces in a laminar flow field as a function of shear stress. The spatial distribution of adherent bacteria on the surface of a radial-flow chamber is monitored via automated videomicroscopy with motorized three-axis stage and focus control, allowing rapid automated measurement of the attached cell density as a function of time and radial position. Intrinsic rate constants for attachment and detachment are defined and estimated by fitting mathematical models to the resulting data. The model for cell attachment accounts for the global transport of cell in the chamber to estimate the cells concentration near the collector surface. The model for cell detachment accounts for heterogeneity in the adhesion energy of the attached cell population. These models yield first-order attachment and detachment rate constants that intrinsically reflect the probabilities of bacteria attachment and detachment as a function of applied shear stress, depending on only the local interactions between the cell and the surface. The validity of each model was tested by statistical analyses of the goodness-of-fit to data that resulted from a study comparing adhesion of Staphylococcus aureus to three different polymeric surfaces of varying surface properties and adhesive protein coatings.

Introduction

Infections of implanted and intravascular devices are potentially life-threatening complications that impede the long-term use of many biomedical devices. Common features of device-centered infections are the impairment of the host defense mechanisms, extreme resistance to antimicrobial therapies, and high mortality rate (Dankert et al., 1986; Gristina et al., 1987; Dougherty, 1988; Gristina et al., 1993). Despite this enormous clinical relevance, the pathogenesis of these infections remains poorly understood.

Device-centered infections typically occur at the site of the biomaterial surface, and bacterial adhesion to the biomaterial is a necessary step in the pathogenesis of these infections (Dankert et al., 1986; Gristina et al., 1987; Dougherty, 1988; Vaudaux et al., 1990). Despite progress in identifying molecular components that are involved in adhesion of some strains, the fundamental physical and molecular mechanisms that govern bacterial adhesion to biomaterial surfaces remain to be elucidated. These mechanisms depend upon the composition and properties of the cell surface, the biomaterial surface, and the conditioning layer of adsorbed proteins on the biomaterial surface (Dankert et al., 1986; Gristina et al., 1987; Dougherty, 1988; Wadstrom, 1989; Vaudaux et al., 1990; Gristina et al., 1993). Elucidation of the mechanisms requires examination of bacterial adhesion under experimental conditions where these properties are well-defined and controllable.

Depending on the device and application, biomaterials may be exposed to a wide range of shear rates. In the human circulation, for example, shear rates can range between 40 s^{-1} and 2,000 s^{-1} for stable Poiseuille flow in vessels (Goldsmith and Turitto, 1986), with much higher shear rates

Correspondence concerning this article should be addressed to Richard B. Dickinson.

possible at vessel entrances, at bifurcations, or, for example, in complex flow patterns such as that of the total artificial heart (NASA Report, 1989). Therefore, stable adhesion requires the ability of the cell to attach *and* to resist detachment when subjected to a fluid shear force, and full quantitative characterization of the "adhesiveness" requires measuring parameters that reflect the probabilities of the attachment and detachment events. Ideally, the measured parameters should be *intrinsic*: they should depend only on the local fluid dynamics and the local interactions between the cell and the surface, and should be independent of arbitrary global experimental parameters, such as incubation time, assay dimensions, and cell concentration in suspension.

Several recent studies have used parallel-plate flow chambers (Wilkinson et al., 1984; Sjollema et al., 1989; Lawrence et al., 1990; Jen and Lin, 1991; van Kooten et al., 1992) or radial-flow chambers (RFCs) (Fowler and McKay, 1980; Crouch et al., 1985; Cozens-Roberts et al., 1990b) to study cell attachment or detachment on surfaces. Flow chambers offer advantages over blind assays, such as incubation of a coverslip or spinning disc in a bacteria suspension then counting the number of attached cells after an arbitrary incubation time. The flow conditions in the flow chambers are well-defined and real-time direct observation and enumeration are possible, thus allowing the attached cell density to be measured as a function of time.

Many studies have measured cell deposition rates in parallel-plate flow chambers (Sjollema et al., 1988, 1989; Jen and Lin, 1991; Busscher et al., 1992; Cowan and Busscher, 1993; Meinders et al., 1994). Under the assumption of first-order attachment kinetics, the deposition rate can be normalized by dividing by the concentration of suspended cells introduced into the chamber to yield an *effective attachment rate constant*. A limitation of this approach, however, is that the actual cell concentration near the surface is generally not known and may vary with the point of measurement. For example, rapid attachment can lead to a downstream depletion of cells near the surface, and slow attachment with cell sedimentation can likewise lead to a downstream accumulation of cells near the surface. Therefore, the measured *effective attachment rate constant* is not an intrinsic measure of the probability of attachment; it is generally a function of the distance from the inlet port as determined by the global cell transport within the chamber and is therefore dependent on the global parameters of the assay. As shown in this article, this caveat can be overcome by estimating the true cell concentration near the surface, thus allowing estimation of an *intrinsic attachment rate constant*.

When *shear-dependent* cell adhesion is of interest, the RFC offers an advantage over the parallel-plate flow chamber in that the shear rate varies continuously with radial distance from the inlet port. However, previous RFC cell-adhesion studies have not measured attachment or detachment kinetics under multiple shear rates simultaneously, thus limiting this advantage.

We describe here a novel methodology and analysis to define and measure *intrinsic rate constants* for attachment and detachment as a function of shear rate, which only depend on the local interactions between the cells and the surface, and the local fluid dynamics. With the aid of automated videomicroscopy and three-axis motorized stage and focus control, the cell density in an RFC was measured as a function of time and radial position by rapidly scanning the surface of the chamber at incremental positions corresponding to varying shear rates. The resulting data for the attached cell density were subsequently interpreted with the aid of phenomenological mathematical models. Fitting numerical solutions of the models to the experimental data via nonlinear least-squares regression yielded estimates of intrinsic attachment and detachment rate constants as functions of shear rate. The validity of each model was tested by a statistical analysis of the goodness of fit to data that resulted from a study comparing adhesion of *Staphylococcus aureus* to three different polymeric surfaces of varying surface properties and adhesive protein coatings (Dickinson et al., 1995b).

Materials and Methods

Buffered media

The fluid media used in all flow experiments was Dulbecco's phosphate-buffered saline (Gibco BRL, Gaithersburg, MD), supplemented with 0.1 mg/mL $MgCl_2$ and 0.1 mg/mL $CaCl_2$, at pH 7.35. (Hereafter, this solution will be referred to as "buffer.") The buffer was filtered and degassed before use.

Bacteria strain and growth conditions

The Newman strain of *Staphylococcus aureus* was used in all experiments. *Staphylococcus aureus* is a common pathogen in device-associated infections (Vaudaux et al., 1985; Herrmann et al., 1988, 1992; Ohtomo and Yoshida, 1988), and the Newman strain is characterized by binding sites for the plasma protein, fibrinogen (Herrmann et al., 1992; McDevitt et al., 1992, 1994). Working cultures were maintained on Mueller-Hinton agar plates. Bacteria were grown overnight in Mueller-Hinton broth, washed twice in buffer, lightly sonicated to separate any clumped cells, then resuspended in buffer at a concentration of 5×10^7/mL for attachment experiments, or at 2×10^8/mL for detachment experiments. As indicated by microscopic observation and by the data (see the titled section Analysis below), this concentration was sufficiently low for insignificant cell–cell interactions.

Proteins

Whole fresh human platelet-poor plasma was prepared from the blood of healthy volunteers by centrifuging ACD (citric acid, final concentration, 5 mM; sodium citrate, 10 mM; and dextrose, 15 mM)-anticoagulated blood for 15 min at 1,500 g; plasma was pooled, aliquoted, and stored at -70°C. Human albumin was purchased from Sigma Chemical Co. (Fraction V, 96–99% pure, Sigma Chemical Co., St. Louis, MO). Human fibrinogen was purchased from Sigma Pharmaceuticals (St. Louis, MO) and further purified using a Gelatin-Sepharose 4B (Pharmacia, Piscataway, NJ) column to remove residual fibronectin. Purity was confirmed by SDS-PAGE.

Radial-flow chamber

The RFC is shown in Figure 1. The design is a modification of that used by Cozen-Roberts et al. (1990b). The RFC

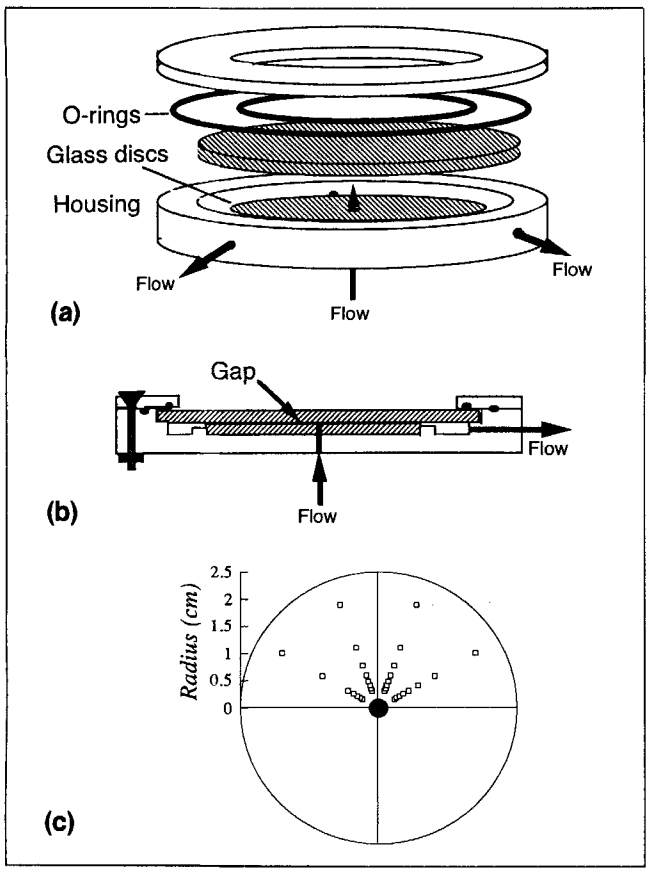

Figure 1. Radial-flow chamber.

(a) Dismantled. (b) Assembled. A Plexiglas chamber houses two optically flat glass discs that are separated by a thin gap. One disc is fixed to the chamber with the inlet port bored in its center and the other disc can be removed and treated with conditions of interest. The fluid flows in through the center of the fixed disc, out radially between the two discs, collects in a surround trough, then flows out through three equally spaced exit ports. (c) Diagram of the scanned regions of radial-flow chamber surface. A region containing eight fields by four fields of the disc was scanned. The fields were spaced radially, the fields at increments inversely proportional to the shear rate. The central circle represents the inlet tubing, which blocked the light path for transmitted light microscopy, and thus limited the minimum measurable radius.

consisted of two optically flat glass discs (Melles Griot, Irving, CA) that were separated by a thin gap (215 ± 5 μm) and housed in a Plexiglas chamber. One disc (50-mm dia., 3-mm thickness) was permanently cemented to the chamber and bored with a 0.080-in.-(2-mm)-dia. inlet port through its center. The second disc (75-mm-dia., 3-mm thickness) was removable to be pretreated with conditions of interest. This disc fit snugly along a ridge within the chamber and was sealed in place with two O-rings. The lid was tightly bolted to prevent leakage and significant deflection of the removable disc from the impinging fluid. The fluid flowed in through the center of the fixed disc, flowed out radially through the gap between the discs, collected in a larger annular trough surrounding the fixed disc, and then flowed out through three equidistant 1.5-mm-dia. exit ports around the circumference of the chamber.

The laminar fluid velocity profile in the RFC has been solved from the Navier–Stokes equation elsewhere (Moller, 1963; Fowler and McKay, 1980) to find the fluid velocity in the radial direction, $v_r(r,z)$ at any radial position, r, and vertical distance from the collector surface, z:

$$v_r(r,z) = \frac{3Q}{\pi r h^2} z(1 - z/h), \tag{1}$$

where Q is the volumetric flow rate, and h is the gap width. Equation 1 implies that the shear rate at the surface of the disc, S, varies inversely with r, as

$$S = \frac{3Q}{\pi r h^2}. \tag{2}$$

In the derivation of Eq. 2, incompressible laminar flow of a Newtonian fluid was assumed, with local Reynolds number, $Re = Q/\pi r\nu$, less than 2,000 (ν is the kinematic viscosity). In the data presented here, the highest flow rate used was 75 mL/min for the detachment experiments such that the radial position corresponding to Re = 2,000 was approximately 0.02 cm, which is smaller than the radius of the inlet port; therefore, laminar flow can be safely assumed.

Flow apparatus

The flow apparatus was similar to that used by Cozens-Roberts et al. (1990b). All tubing was 1/8″ ID Silastic silicone tubing (Dow Corning, Midland, MI) except where otherwise specified, and flow was regulated with two-way and three-way stopcocks with luer lock adapters (Rainin, Woburn, MA). A constant head tank (CHT) (consisting of a separatory funnel (250 mL for attachment; 1 L for detachment) with stopcock, a rubber stopper with single hole, and glass capillary tubing extending beneath the fluid level) was used as a constant-pressure feed source for the fluid, and a variable flow rate controller (VFRC) was used to control the volumetric flow rate. A syringe with three-way luer lock valve was placed in the tubing between the VFRC and the RFC. The three exit ports of the RFC were controlled by two-way stopcocks with luer lock adapters, connected to 1/16-in. (1.6-mm)-ID Tygon tubing that joined at a cross-junction flow connector (Glass-Filled PTFE Cross, Rainin, Woburn, MA), then led to a waste container.

Before operation, all tubing was equilibrated with buffer and air bubbles were removed by using the syringe to manually pump the fluid through the lines at high shear rates. The stopcock of the CHT was opened to drain cell-free buffer from the CHT and the cell suspension was added. The VFRC was fully opened until cells appeared at a significant concentration in the RFC, then the VFRC was adjusted to maintain a volumetric flow rate of 2.0 mL/min, corresponding to measurable shear rates between about 35 s^{-1} and 200 s^{-1}. A constant flow rate was maintained by counting the number of drops per second into the waste flask. (The flow rate was previously calibrated by measuring the accumulated volume over a known time period.)

The flow apparatus was modified for the detachment experiments in the following ways: an additional syringe with three-way luer lock valve was inserted between the VFRC

and RFC. Another three-way valve allowed flow to be switched from the waste container to a flow-fluctuation suppresser (FFS) (consisting of a sealed flask with an inlet capillary tube extending just below the stopper, and the exit tube extending below the fluid level in the flask). Tubing connected FFS to a peristaltic pump, then the peristaltic pump to an additional capillary tube entering the CHT. Eight mL of bacteria suspension (2×10^8/mL) was introduced into the RFC without introducing air bubbles by first removing one syringe to draw in the cell suspension, reattaching the syringe, setting the luer lock valves to connect the adjacent syringes, then pumping the suspension back and forth to displace any interceding air in the line between the syringes, ending with approximately 6 mL of the cell suspension in one syringe. The valve configuration was then set to connect this syringe with the RFC, and the cell suspension was then injected into the RFC. The cells were allowed to settle for 10 min before initiating a very slow flow rate (<1 mL/min) to purge the chamber of all remaining suspended cells between the syringes and the trough of the RFC. Detachment experiments were then conducted at a flow rate of 75 mL/min, corresponding to measurable shear rates between 1,500 and 7,000 s^{-1}. During the first few minutes of detachment, the initial cell-rich fluid was collected in the waste flask to flush all suspended and early-detaching cells from the circuit. The circuit was then closed and the peristaltic pump was used to recirculate buffer to the CHT. Although a closed circuit allowed detaching cells to recirculate through the chamber, the large volume of buffer (>1 L) containing a relatively small number of cells maintained a negligible cell concentration in the circulating fluid. The FFS kept pressure in the lines steady by preventing pump-induced pressure fluctuations, and the pump speed was monitored to maintain a constant pressure in the CHT.

The RFC and flow apparatus were disassembled and thoroughly cleaned in disinfectant soap between uses to avoid contamination.

Polymers

To obtain the example data shown here, attachment and detachment kinetics were observed on three different polyurethanes synthesized in our laboratory. Complete results of this study are presented elsewhere (Dickinson et al., 1995b). The materials were chosen for their similar overall chemistry, but distinct surface properties. These included a "base" polyetherurethane (PEU-B) (polytetramethylene hard segment, methylene diphenylene diisocyanate hard segment, 1,4-butanediol chain-extender), and two ionomer derivatives of the base material: a positively charged aminated polyetherurethane (PEU-N) (obtained by substituting the butanediol chain-extender with a diol containing a cationic methyl quaternized amine side chain), and a negatively charged polyether-urethane ionomer (PEU-S) (obtained by substituting the urethane hydrogen with an anionic pendant sulfonate group). Synthesis and characterization of these materials are described elsewhere (Grasel, 1987; Grasel and Cooper, 1989; Hergenrother, 1991; Goddard and Cooper, 1994).

Disc preparation

The discs were pretreated by first soaking overnight in a concentrated chromium trioxide/sulfuric acid solution (25-mL Monostat Chomerge per 9-lb (4.1-kg) concentrated sulfuric acid, Baxter Diagnostics, Inc., McGaw Park, IL), then soaking twice for one hour in twice-distilled deionized water, twice for one hour in methanol, and dried one hour in a vacuum oven. Polymer-coated discs were prepared by spin coating a polymer film onto the discs from 1% *N,N*-dimethylacetamide solution, allowing the discs to dry in a vacuum oven (60°C, ~10 torr), then equilibrating overnight in buffer. This method generally yielded smooth, uniform polymer films, as could be determined macroscopically and microscopically. Before use in adhesion experiments, discs were incubated overnight in buffer, then pretreated in one of four ways: (1) 2 h in buffer alone as a bare control; (2) 1 h in 0.020 μg/mL fibrinogen solution (in buffer), then 1 h in 0.5% human albumin in buffer; (3) 1 h in buffer, then 1 h in 0.5% human albumin solution; or (4) 2 h in 1% platelet-poor plasma solution. (Hereafter, these treatments are referred to as "Bare," "Fg," "HSA," and "PPP," respectively.) During treatment, the discs were swirled in the protein solutions (or control buffer) on a rotating platform. After the treatment period, the protein solution was replaced with buffer.

Automated videomicroscopy

An automated videomicroscopy and image-analysis system was used to achieve rapid counts of attached bacteria over the surface of the treated disc in the RFC as a function of time. This system consisted of a Nikon Diaphot inverted microscope (40X Extra Long Working Distance Objective) with motorized stage (0.1-μm spatial resolution) with associated three-axis stage and focus controller (LUDL Electronics Products Ltd., Hawthorne, NY), a Dage NC-65 Newvicon video camera (Dage MTI, Inc., Michigan City, IN), a Sony SVO-9500MD Videocassette Recorder (VCR) with Trinitron color monitor (Sony Medical Systems, Montvale, NJ), and a Gateway2000 4DX2-66E minicomputer (Gateway 2000, North Sioux City, SD) with OFG frame-grabbing board (640×480 pixels) (Imaging Technologies, Bedford, MA) and Optimas image analysis software (Bioscan, Inc., Edmonds, WA). The VCR and the motorized stage/focus controller were connected on-line to the minicomputer via RS232C serial connections, and analog video input from the video camera or VCR was digitized by the frame-grabbing board and processed by Optimas software functions, thus allowing rapid and automated operation of microscope field selection, image archiving, and image processing.

Data acquisition

Data were acquired with the aid of two programs written in the Optimas ALI (Analytical Language for Images) programming language. In the first program, the planar x, y, and z coordinates of a wedge-shaped region of the RFC disc were first defined and stored, then 32 fields of the region were recursively scanned using automated motorized and focus control, as images of the scanned fields were stored on videotape. As shown in Figure 1c, the scanned region consisted of four azimuthal positions for each of eight of radial positions, which were spaced at incremental distances inversely proportional to the radius (hence proportional to the shear rate). A second program then replayed the taped image sequences, processed the images to remove any background

shading effects, counted the number of attached cells (excluding background noise based on size discrimination), and then stored the cell counts in a spreadsheet file. Separating image acquisition and image analysis into two steps maximized the rate of data acquisition such that the rate was only limited by the stage movement velocity, allowing images to be acquired at an overall rate of approximately 20 fields per minute, with the four fields of each radial distance being scanned over about 10 s. This high image acquisition rate was essential to allow cell counts in multiple fields, and thus a statistically significant measurement of the cell density as a function of time and radial position. Observations of cell clumps were uncommon and considered insignificant relative to the number of individual bacteria.

The surface density of attached cells was measured by averaging the number of cells in the four azimuthal fields, and dividing this average by the area per field (~ 0.032 mm^2). The cell-counting procedure could not distinguish cell-sized dust particles on microscope or video camera surfaces or anomalies on the biomaterials surface from bacteria. Therefore, during the detachment experiments, each field was counted twice before bacteria were introduced into the chamber, after which the average of the two counts was subtracted from subsequent cell counts. The calculations for the attachment experiments, however, did not depend on the initial attached cell density (only the rate of increase, as discussed below); therefore, quantifying this small background "noise" was unnecessary.

Estimation of settling velocity

The settling velocity, V, was estimated by filling the chamber at a cell concentration of $c_0 = 2 \times 10^7$ cells/mL, and focusing the objective 5 μm above the surface. All cells within a volume immediately above and including the surface were then viewed and counted as the bacteria settled to the surface. The Optimas programs just described were then run to count cells within this volume as a function of time. For a rapidly binding surface such as bare glass where the flux of cells due to binding is greater than the settling velocity, then the number of cells within this volume per unit area, N, increases with a constant rate equal to Vc_0. V was obtained from a linear regression estimate of the slope of N vs. time, then divided by c_0, yielding a value of 3.5×10^{-4} cm/min.

Analysis

Attachment

Figure 2 shows example data for the attachment of *Staphylococcus aureus* to Fg- and HSA-coated PEU-N. The attached cell density, $c_s(r, t)$, is plotted vs. time, t, at a radial position, r, corresponding to a shear rate of about 100 s^{-1}. These results were consistent for all surfaces measured for shear rates up to 200 s^{-1}, in that c_s increased linearly with t. This observation implies that the rate of change $c(r, t)$, and thus the net flux of cells to the surface, was constant in time. A constant net flux suggested that (1) the spatial distribution of cells in suspension, $c(r, z)$, was at a steady state; (2) the attached cell density was sufficiently low as to not influence the attachment of new cells; and (3) the rate of detachment was negligible relative to the rate of attachment (otherwise,

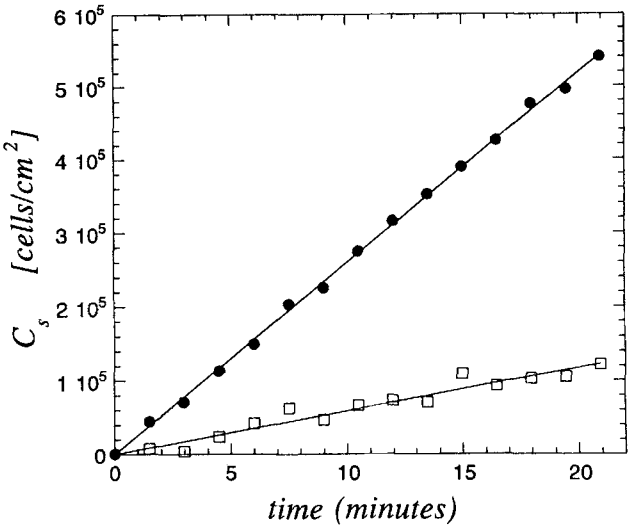

Figure 2. Example data for cell attachment kinetics.

The attached cell density of attached *Staphylococcus aureus* is plotted vs. time on the aminated polyurethane (PEU-N) pretreated in albumin (circles) or human plasma (squares). The values were calculated from the average of cell counts, four fields at a radial position corresponding to approximately 100 s^{-1}. The solid lines are the linear least-squares solution fitted to the data.

dc_s/dt would not be constant because the rate of detachment is expected to be an increasing function of c_s). Under these conditions, the flux of cells to the surface can be assumed to be proportional to the concentration of cells introduced into the chamber, c_0, that is,

$$\frac{dc_s(r,t)}{dt} = k_{\text{eff}}(r)c_0, \tag{3}$$

where $k_{\text{eff}}(r)$ is the *effective attachment rate constant* at radius, r. The solution to Eq. 3 is simply

$$c_s(r,t) = k_{\text{eff}}(r)c_0 t. \tag{4}$$

Therefore, $k_{\text{eff}}(r)$ can be obtained by dividing the slope of $c_s(r, t)$ vs. t by c_0.

Although measuring $k_{\text{eff}}(r)$ may provide useful overall comparison of attachment rates between experimental conditions, it inadequately reflects the dependence of attachment on shear rate; k_{eff} can depend on r not only because the probability of cell attachment depends on $S(r)$, but also because the number of cells (cell concentration) near the surface that are available for attachment may vary with r. Because the rate of attachment is expected to be proportional to the concentration of cells "near" the surface, k_{eff} depends on the global transport of cells within the chamber and therefore is not an intrinsic parameter.

Assuming that the actual cell concentration, $c(r, z)$, can be defined as a continuous function of r and z, a more descriptive model for attachment is

$$\frac{dc_s(r,t)}{dt} = k_+(r)c(r, z \sim 0), \tag{5}$$

where $k_+(r)$ is the *intrinsic attachment rate constant* that depends only on the local interactions between the cell and the surface. Combining Eqs. 3 and 5, k_{eff} is related to k_+ by the relation

$$k_{\text{eff}}(r) = k_+(r)\, c(r, z \sim 0)/c_0 \tag{6}$$

Therefore, if $k_{\text{eff}} \neq 0$, then $k_{\text{eff}} = k_+$ if and only if $c(r, z \sim 0) = c_0$. Estimating $k_+(r)$ from $k_{\text{eff}}(r)$ requires the additional knowledge of $c(r, z)$, which, unfortunately, depends on $k_+(r)$ itself.

To proceed, we construct a mathematical model for the transport of cells in the RFC to predict $c(r, z)$ and $k_{\text{eff}}(r)$, which is based on a simple two-parameter phenomenological expression for $k_+(r)$. One parameter represents a base value of k_+ in the limit of zero shear; the other reflects the dependence of k_+ on $S(r)$. The model solution can then be fitted to the experimental data for $k_{\text{eff}}(r)$ to obtain estimates for these two parameters.

Because we wish k_+ to reflect all interactions between the cell and the surface with as few unknown or ill-defined parameters as possible, we apply the so-called *surface force boundary layer approximation* for colloid deposition (Ruckenstein, 1975; Bowen et al., 1976; Dabros and van de Ven, 1982; Adamczyk et al., 1983; Chari and Rajagopalan, 1985), where the z direction is segregated into two regions: a "bulk" region where interactions between the cell and surface are insignificant, and an "interaction" region of distance, Γ, where all interactions between the cell and the surface, including additional hydrodynamic drag on the cell from the presence of the surface (Brenner, 1961), are assumed to occur. The flux of cells in the z direction, $J_z(r, z)$, is assumed uniform across Γ, and proportional to the cell concentration at Γ with proportionality constant k_+. The net flux *toward* the surface $(-J_z)$ is then equal to the rate of accumulation:

$$\frac{dc_s(r,t)}{dt} = -J_z(r,\Gamma) = k_+(r)c(r,\Gamma). \tag{7}$$

For the bulk region, because the fluid velocity is zero in the z direction, only diffusion and gravitation contribute to the cell flux:

$$J_z(r,z) = -D\frac{\partial c}{\partial z} - Vc \qquad (z \geq \Gamma), \tag{8}$$

where D is the cell diffusion coefficient, and V is the settling velocity. Therefore, assuming negligible diffusion in the x direction relative to convection, the continuity equation for $c(r, z)$ at steady state provides

$$0 = -v_r(r,z)\frac{\partial c}{\partial r} + D\frac{\partial^2 c}{\partial z^2} + V\frac{\partial c}{\partial z} \qquad (z \geq \Gamma). \tag{9}$$

The lower boundary condition is obtained by matching the fluxes at Γ, which, upon combining Eqs. 7 and 8 is

$$D\frac{\partial c(r,z)}{\partial z}\Big|_\Gamma + Vc(r,\Gamma) = k_+(r)c(r,\Gamma). \tag{10}$$

At this point we must propose a phenomenological expression for k_+ as a function of $S(r)$. Assuming cells must cross through a transitional energy state when moving between unattached and attached states, we hypothesize that k_+ obeys an Arrhenius-type law (Bromberg, 1984):

$$k_+(S) = A\exp(-E_a(S)/\kappa T), \tag{11}$$

where E is the free-energy difference of the transitional energy state and the free state (*activation energy*), A is a constant (*preexponential factor*), κ is Boltzmann's constant, and T is the absolute temperature. As a first approximation, we assume E_a is a linear function of S,

$$E_a(S) = E_0 + E_1 S \tag{12}$$

This assumption yields

$$k_+ = k_{+0}\exp\left(\delta\frac{S}{S_{\min}}\right) \tag{13}$$

where k_{+0} is the *base attachment rate constant*, that is, the hypothetical zero-shear limit of k_+, given by

$$k_{+0} \equiv A\exp(-E_0/kT). \tag{14}$$

Here, $S_{\min} \equiv S(R)$ is the minimum shear rate, and $\delta \equiv E_1 S_{\min}$ is the *attachment shear-sensitivity coefficient*.

To reduce the number of independent parameters and facilitate subsequent numerical analysis, Eqs. 1 and 9 are made dimensionless and combined to obtain a dimensionless partial differential equation for dimensionless cell concentration, $u = c/c_0$:

$$u_x = \frac{x}{\beta(y - \eta y^2)}(u_{yy} + u_y) \tag{15}$$

where the new dimensionless spatial variables are $x = r/R$, and $y = zV/D$. The term β is a dimensionless flow parameter defined by

$$\beta = \frac{S_{\min}R}{V}\left(\frac{D}{RV}\right)^2 \tag{16}$$

and is essentially the ratio of convective velocity to settling velocity, multiplied by the square of the inverse of the Peclet number, $Pe = RV/D$; $\eta = D/Vh$ is the inverse of the Peclet number of sedimentation. Upon combining Eqs. 10 and 12, the dimensionless boundary condition at the surface is

$$u_y(x,\gamma) = (\alpha e^{-\delta/x} - 1)u(x,\gamma), \tag{17}$$

where two additional dimensionless groups are defined as

$$\alpha = k_{+0}/V \tag{18}$$

$$\gamma = \Gamma V/D, \tag{19}$$

which are the *dimensionless base attachment rate constant*, and the *dimensionless interaction distance*, respectively.

To this point, we have ignored the upper boundary condition. Under conditions where cells near the center of the gap are convected out of the chamber much faster than they can diffuse or settle to the surface, we expect the upper surface of the chamber to have no effect on the cell concentration near the lower surface. Mathematically, if $(3Q/\pi Rh^2) \gg Vh$ and $D/V \gg h$, then the upper boundary is effectively at infinite distance away from the lower surface with respect to cell transport in the z direction. Therefore, we can set the upper boundary condition either as

$$u(x, y \gg 1) = 1 \tag{20}$$

or as

$$u_y(x, y \gg 1) = 0. \tag{21}$$

Boundary conditions 20 and 21 equivalently reflect the situation where the bulk cell concentration is undisturbed far from the lower surface. For numerical analyses, Eq. 20 is assumed and is justified by the results presented below.

Detachment

We also seek an intrinsic parameter that reflects the probability of bacteria detachment. We first try a similar approach as the attachment model, by assuming first-order kinetics with rate constant, k_-, which is equivalent to the probability per unit time of a cell detaching. If k_- is constant with time, and uniform among the population of attached cells, then the rate of change in attached cell density, c_s, is given by

$$\frac{dc_s}{dt} = -k_- c_s. \tag{22}$$

For initial cell density, c_{s0}, the solution to Eq. 22 is

$$c_s(t) = c_{s0} e^{-k_- t}. \tag{23}$$

As shown in the example data in Figure 3 for *Staphylococcus aureus* detaching from HSA-coated and Fg-coated PEU-S, the data for $c_s(t)$ showed decay behavior from the initial value, c_{s0}, but regression fits of Eq. 23 to the data displayed systematic deviation of the data from the model. The data indicate a faster rate of detachment at early time and a slower rate of attachment at larger times than that predicted by a pure exponential decay model. This discrepancy was consistently observed for all tested surfaces. A likely explanation is that the probability of detachment was not uniformly distributed over the cell population; all cells may not have had the same value of k_-. To explore this possibility, we define $p(k_-, t)$ as the probability that an initially attached cell with detachment probability per unit time, k_-, remained attached at time t. The rate of change of $p(k_-, t)$ is then given by

$$\frac{dp(k_-, t)}{dt} = -k_- p(k_-, t) \tag{24}$$

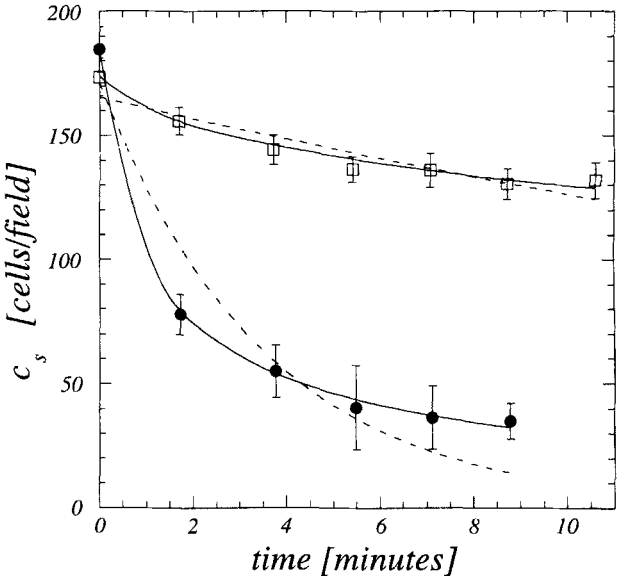

Figure 3. Example data for cell detachment kinetics.
Example data for the attached cell density, c_s, of detaching *Staphylococcus aureus* on Fg-coated (squares) and HSA-coated PEU-S (circles) are plotted vs. time. The dashed line is the least-squares regression fit of the two-parameter exponential decay model, whereas the solid line is the fit of the more general three-parameter model. For these two examples, the regression analyses for the two-parameter model yielded $k_- = 0.027 \pm 0.005$ min^{-1}, and $k_- = 0.28 \pm 0.06$ min^{-1}, respectively, and for the three-parameter model, $\bar{k}_- = 0.55 \pm 0.5$ min^{-1}, $\sigma = 1.9 \pm 0.2$, and $\bar{k}_- = 0.0094 \pm 0.0059$ min^{-1}, $\sigma = 2.4 \pm 0.9$, respectively.

with solution

$$p(k_-, t) = p_0(k_-) e^{-k_- t}, \tag{25}$$

where $p_0(k_-)$ is the initial distributions of k_- among the attached cell population at the initiation of flow. Term $c_s(t)$ is then equal to the integral over all possible values k_-, multiplied by the initial cell density, c_{s0}, that is,

$$c_s(t) = c_{s0} \int_0^\infty p(k_-, t)\, dk_-. \tag{26}$$

Combining Eq. 26 with Eq. 25, we have

$$c_s(t) = c_{s0} \int_0^\infty p_0(k_-) e^{-k_- t}\, dk_-. \tag{27}$$

In the limit where k_- is uniformly distributed among all the cells, say with $k_- = \bar{k}_-$, then $p_0(k_-)$ is the delta function, $\delta(k_- - \bar{k}_-)$, and Eq. 27 becomes equivalent to Eq. 22, with $k_- = \bar{k}_-$.

We seek a distribution for $p_0(k_-)$ with a meaningful physical basis that predicts a function $c_s(t)$ that adequately reflects the data but minimizes the number of unknown parameters. Similar to the attachment model, we assume the detachment rate constant obeys an Arrhenius relation of the form

$$k_- = Ae^{-E/\kappa T}, \tag{28}$$

where E is the *energy of adhesion*, defined here relative to the energy of the transition state between the attached and detached states: E is the energy the cell must overcome to detach. We note that heterogeneity in E may result from any probabilistic variations in the state of the adhesion. These variations may result from the discrete cell-surface interactions: for example, the number of cell receptors bound to adsorbed proteins on the surface may vary from cell to cell, even if each cell retained the same total number of receptors (Cozens-Roberts et al., 1990b). The simplest assumption is that $E/\kappa T$ has a normal distribution with mean $< E > /\kappa T$, and variance σ^2. Equation 28 can then be rewritten as

$$k_- = \bar{k}_- e^{-\epsilon}, \tag{29}$$

where $\epsilon = (E - < E >)/\kappa T$, and $\bar{k}_-$ is the *mean-energy detachment rate constant*, that is,

$$\bar{k}_- = Ae^{-< E > /\kappa T} \tag{30}$$

and σ is termed the *adhesion energy heterogeneity coefficient*.

Given that ϵ is normally distributed, $\epsilon \sim N(0, \sigma)$, then k_- has a lognormal distribution, $k_- \sim LN(\ln(\bar{k}_-), \sigma)$, that is,

$$p_0(k_-) = \frac{1}{k_- \sigma\sqrt{2\pi}} \exp\left(\frac{-(\ln(k_-) - \ln(\bar{k}_-))^2}{2\sigma^2} \right). \tag{31}$$

Therefore, from Eq. 27, the cell density is given by

$$c_s(t) = c_{s0} \int_0^\infty e^{-k_- t} \frac{1}{k_- \sigma\sqrt{2\pi}} \exp\left(\frac{-(\ln(k_-) - \ln(\bar{k}_-))^2}{2\sigma^2} \right) dk_-. \tag{32}$$

As σ approaches 0, then $p_0(k_-)$ approaches $\delta(k_- - \bar{k}_-)$, yielding

$$c_s(t) = c_{s0} e^{-\bar{k}_- t}. \tag{33}$$

Hereafter, Eq. 33 will be referred to as the *two-parameter* detachment model (considering c_{s0} to be an additional parameter to be estimated in the regression analysis) and Eq. 32 as the *three-parameter* detachment model. Statistical comparison of these two models is discussed below.

Results

Attachment

To obtain numerical solutions for Eq. 15, estimated values of fixed parameters β, η, and γ were required, leaving α and δ to be fitted from the data. The cell diffusion coefficient was estimated from the Stoke–Einstein equation (Cussler, 1984).

$$D = \frac{\kappa T}{6\pi\mu R_c}, \tag{34}$$

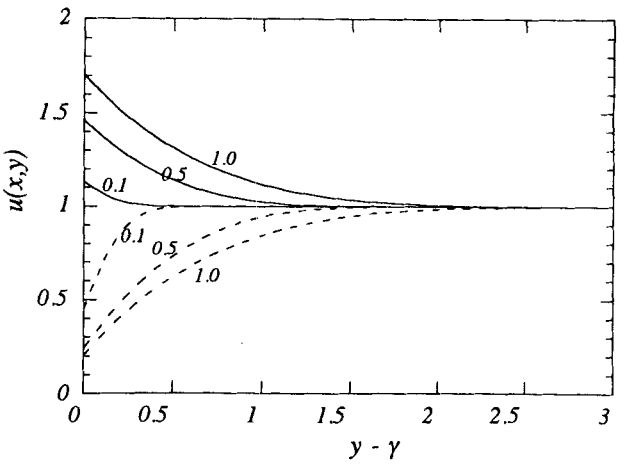

Figure 4. Attachment model predictions dependence of bulk cell concentration on dimensionless attachment rate constant, $\alpha = k_{+0}/V$.

The dimensionless cell concentration, $u(x, y)$, is plotted vs. dimensionless vertical distance, y, for three different dimensionless radial positions, $x = 0.1$, 0.5, 1.0, and for $\alpha = 0.0$ (solid lines) and $\alpha = 10.0$ (dashed lines). For $\alpha < 1$, cells accumulation near the surface is observed, and for $\alpha > 1$, the cell depletion is observed. Also note that even for extreme values of α, u approaches 1.0 for $y \gg 1.0$.

where κ is Boltzmann's constant (1.38×10^{-16} erg/K), T is the absolute temperature ($T = 298$ K), μ is the fluid viscosity (0.01 poise), and R_c is the cell radius (0.5 μm), resulting in $D = 3 \times 10^{-7}$ cm^2/min. The settling velocity was estimated experimentally to be $V = 3.5 \times 10^{-4}$ cm/min (see the section titled Materials and Methods). Taking $R = 1.8$ cm, then $\beta = 3.0$. Assuming the interaction distance, Γ, was slightly larger than $R_c = 0.5$ μm, and we chose $\Gamma = 0.7$ μm, yielding $\gamma = 0.08$. Finally, $h = 215$ μm implied $\eta = 0.035$.

Equation 15 was solved numerically using the method of lines. The y domain was approximated with a finite difference scheme at forty nodes, $\{y_i\}$, and the resulting system of ordinary differential equations, $\{dy_i/dx\}$, was numerically integrated using an explicit fourth-order Runge–Kutta scheme with step-size control based on the formulas of Dormand and Prince (1980). The numerical solution for $u(x, y)$ is plotted in Figure 4 for three values of x and for both large and small values of $\alpha = k_+/V$ (here, $\delta = 0$). As this plot shows, a value of k_+ larger than V (that is, $\alpha > 1.0$) results in depletion of cells near the surface for increasing x. Conversely, $k_+ < V$ (that is, $\alpha < 1.0$) results in accumulation of cells near the surface for increasing x. Also note from Figure 4 that u approaches unity for large y, indicating that the conditions specified by Eqs. 20 and 21 are valid.

The dependence of k_{eff} on a varying $c(z, y \sim 0)$ is shown in Figure 5, where the ratio of effective to intrinsic attachment rate constants, k_{eff}/k_+, is plotted vs. dimensionless radial distance, x, for several values of α. For $\alpha > 1$, k_{eff} is less than k_+, implying that when the attachment rate is greater than the settling rate, cell depletion near the surface ($u(x, \gamma) < 1$) results in a decrease in k_{eff} relative to k_+ (c.f. Eq. 6). Conversely, for $\alpha < 1$, cell accumulation near the surface ($u(x, \gamma) > 1$) results in an increase in k_{eff} relative to k_+.

Figures 6a and 6b show the sensitivity of the model predic-

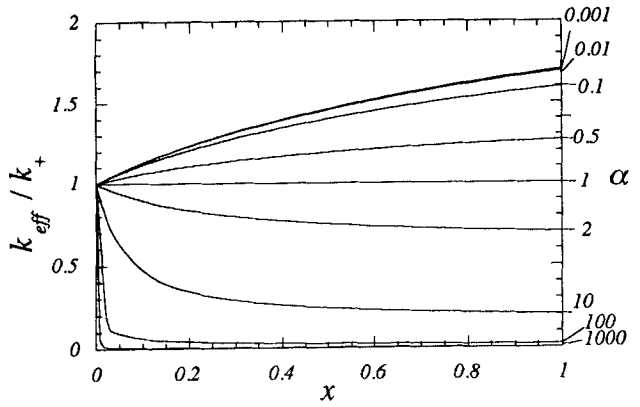

Figure 5. Model predictions for the effect of cell depletion or accumulation on k_{eff}.

The ratio of the *effective attachment rate constant*, k_{eff}, to the *intrinsic attachment rate constant*, k_+, are plotted vs. dimensionless radius, x. The curves correspond to for values of α ranging from 10^{-3} to 10^2 to show the effect of accumulation ($\alpha < 1$) or depletion ($\alpha > 1$) on the effective attachment rate. For $\alpha < 1$, cells accumulate at increasing x, leading to an increase in k_{eff} relative to k_+. Conversely, for $\alpha > 1$, cell depletion results in a decrease in k_{eff} relative to k_+. Note that for $\alpha = 1$, the attachment rate constant equals the settling velocity, leading to neither accumulation nor depletion.

tions to δ for large and small values of α, respectively. Comparison of $k_{eff}(S)$ to $k_+(S)$ shows that k_{eff} remains close to k_+ for large S (small r), but deviates considerably from k_+ at small S (large r). In fact, as shown in Figure 6a, the model predicts a maximum in k_{eff} at intermediate shear rates when $\delta > 0$, resulting from cell accumulation at small r where k_+ is small, but cell depletion at large r where k_+ is large. Conversely, as shown in Figure 6b with $\alpha < 1$, no maximum is predicted, and k_{eff} rapidly becomes much larger than k_+ for small S (large r). In either case, k_{eff}/V approaches unity as S approaches zero, corresponding to the hypothetical situation of infinite radius.

The chosen values for dimensionless parameter β and γ involved rough estimates. Parameter β depends on the cell diffusion coefficient, which was estimated with the Stokes–Einstein equation, assuming hydrodynamic radius of 0.5 μm. The actual hydrodynamic radius may differ significantly from this value; for example, the hydrodynamic radius of a "hairy" cell may be significantly larger than of a "smooth" cell of the same size. The interaction distance, Γ, was chosen to be on the order of a cell radius, where long-range and hydrodynamic interactions between the cell and the surface are expected to become important, but this is really an order of magnitude estimate. To determine whether uncertainty in the fixed parameters adversely affects the model predictions, the sensitivity of the solution to Eq. 15 to these parameters was established. In Figures 7a and 7b, solutions for k_{eff} are plotted vs. S for a range of reasonable values of β and γ, respectively, for both large and small values of α. As these plots indicate, the model predicts k_{eff} to weakly depend on β and γ, suggesting that minimal error in evaluating k_{eff} is propagated by errors in estimating β or γ.

To determine $k_+(S)$ from the data for $k_{eff}(s)$, the two fitted parameters, k_{+0} (that is, α) and δ, were estimated by fitting the numerical solution of Eq. 15 to the experimental

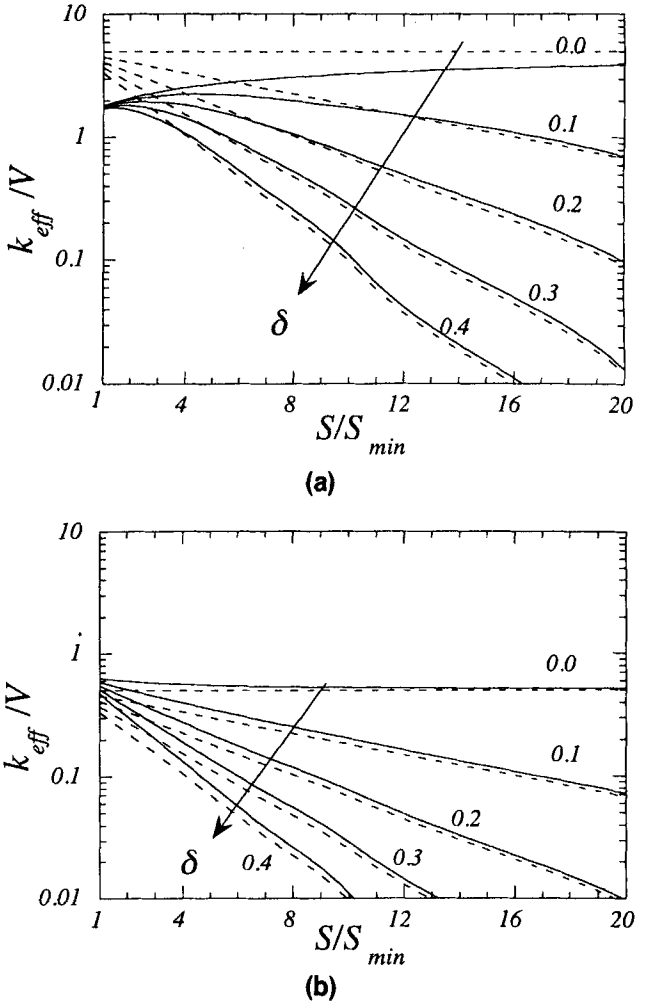

Figure 6. Effect of the *attachment shear-sensitivity coefficient*, δ, on model predictions of the *effective attachment rate constant*, k_{eff}.

k_{eff} (solid lines) and the *intrinsic attachment rate constant*, k_+ (dashed lines), are plotted vs. shear rate, S. The curves correspond to various values of δ at two fixed values of $\alpha = k_{+0}/V$: (a) $\alpha = 5.0$, and (b) $\alpha = 0.5$.

data for $k_{eff}(r)$ via nonlinear least-squares regression. Figure 8 shows an example plot of k_{eff} vs. S for the attachment of *Staphylococcus aureus* to the HSA-coated and bare PEU-N surfaces. The fitted solutions are shown for k_{eff} and $k_+(S)$ based on Eq. 15 with regression estimates of k_{+0} and δ. In this example, k_{+0} was higher and δ was smaller on the bare surface relative to the HSA-coated surface.

To qualitatively demonstrate the goodness-of-fit of the model to the data over a range of experimental conditions, the residuals of the regression fits are plotted in Figure 9 corresponding to several sets of experimental data testing a range of surface properties and attachment rates. These data resulted from a study examining the attachment of *Staphylococcus aureus* to three different polyurethanes under four different pretreatments (see the section titled Materials and Methods) (Dickinson et al., 1995b). The uniform scatter of residuals about zero for all of the shear rates suggests a lack of systematic deviation of the model from the data. This qual-

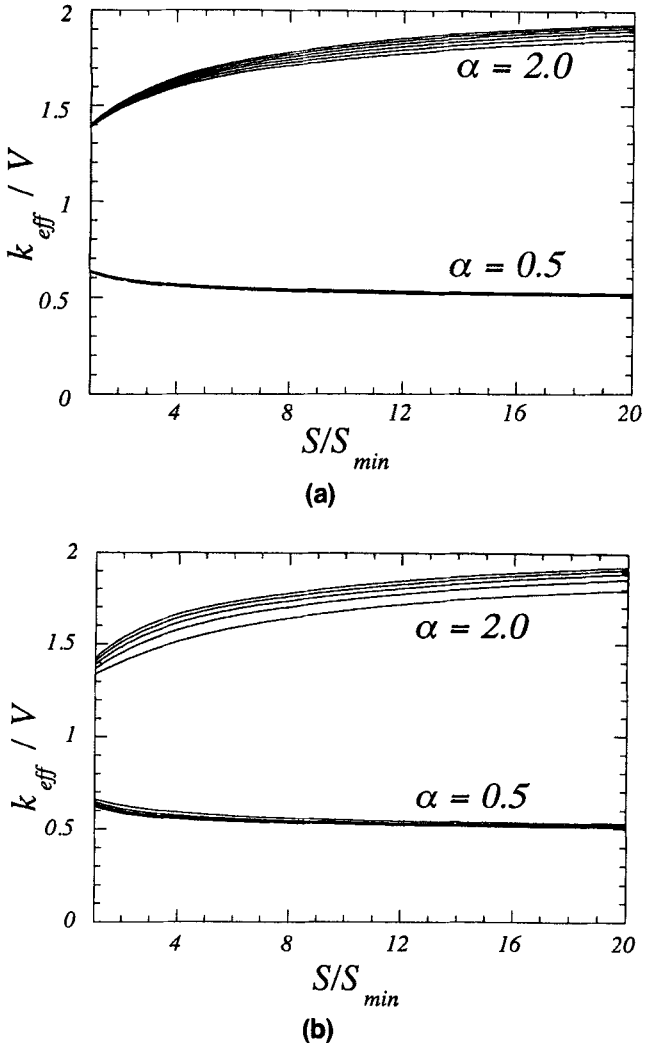

Figure 7. Sensitivity of attachment model solutions to fixed parameters.

Model predictions for the *effective attachment rate constant*, k_{eff} are plotted vs. *shear rate*, S, for five values of (a) the *dimensionless interaction distance*, γ, ranging linearly in value between 0.05 and 0.5 and (b) the *dimensionless flow parameter*, β, ranging linearly between 1.0 and 5.0, for fast attachment ($\alpha = 0.5$) and slow attachment ($\alpha = 2.0$), respectively.

itative observation was confirmed with a statistical goodness-of-fit test of the regression analysis. An analysis of the variance of the residuals was performed by considering data for all samples at any given radial position number as replicated tests of the model at one *regressor* point. The *total residual sum-of-squares* was decomposed into a *lack-of-fit sum-of-squares* and a *replication sum-of-squares*, which was equal to the total sum of squares of the residuals about their averages at each radial position (Bates and Watts, 1988; Seber and Wild, 1989). The ratio of the *lack-of-fit mean square error* over the *replication mean square error* was then compared to the F distribution, where a small p-value would indicate a significant lack of fit. The pooled data from 12 experimental conditions and 8 radial positions yielded a p-value of 0.47, thus quantitatively confirming no systematic deviation of the model from the data.

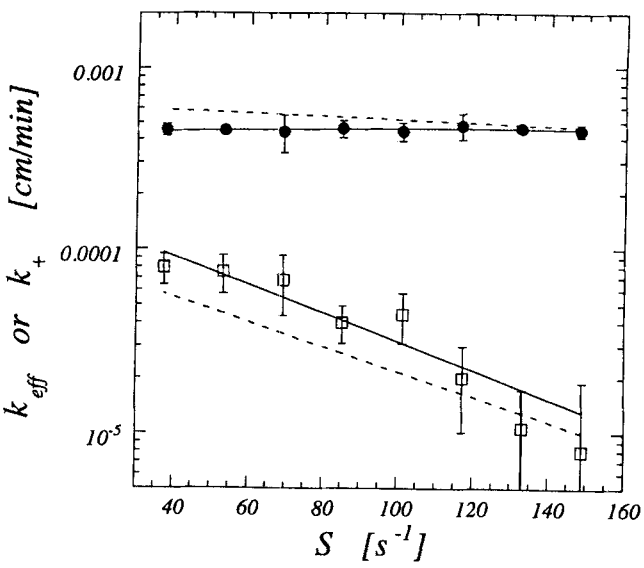

Figure 8. Example application of attachment model.

Example data for the *effective attachment rate constant*, k_{eff}, are plotted vs. shear rate, S, for *Staphylococcus aureus* on HSA-coated PEU-N (squares), and on bare PEU-N (circles). The solid lines represent fits of the model solutions for $k_{eff}(S)$ to the experimental data via nonlinear least-squares regression. The dashed lines represent the *intrinsic attachment rate constant*, $k_+(S)$. The regression analyses yielded values of $k_{+0} = 1.02 \pm 0.42 \times 10^{-4}$ cm/min, $\delta = 0.59 \pm 0.19$ for the HSA-coated surface, and $k_{+0} = 6.30 \pm 0.10 \times 10^{-4}$ cm/min, $\delta = 0.068 \pm 0.006$ for the bare surface.

Detachment

Figure 10 shows the sensitivity of the model predictions for $c_s(t)$ to values of $\bar{k}_-$ and σ, based on numerical integration of Eq. 27. As shown in Figure 10a, large values of $\bar{k}_-$ result

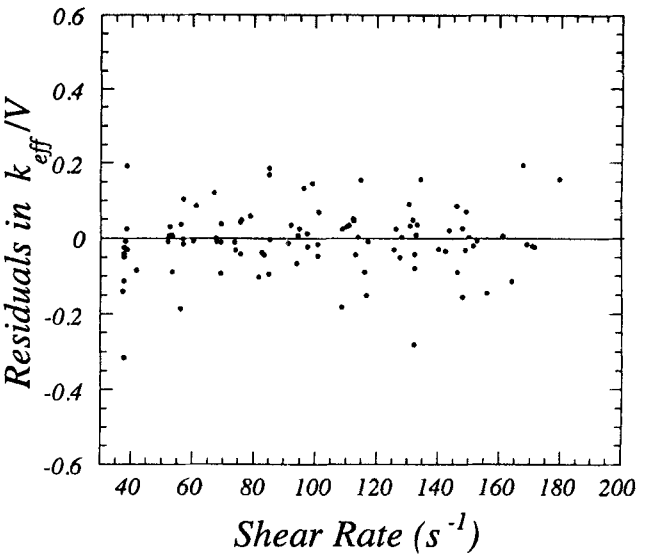

Figure 9. Goodness of fit of the attachment model.

The residuals from the nonlinear regression analysis are plotted vs. shear rate for the attachment of *Staphylococcus aureus* to the three different polyurethane biomaterials (PEU-B, PEU-N, and PEU-S) under the four different pretreatment conditions (Bare, HSA, Fg, and PPP), showing uniform scatter of the residuals about zero, and indicating a good fit of the model to the data.

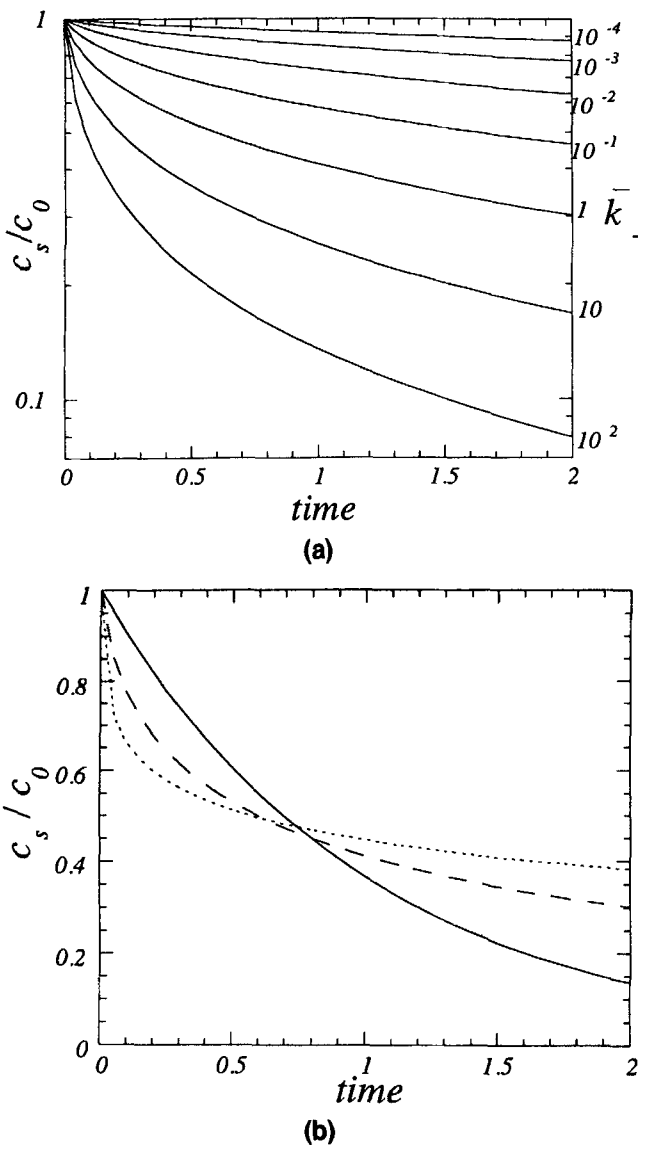

Figure 10. Sensitivity of the detachment model to fitted parameters.

Model predictions for attached cell density c_s (scaled to the initial density, c_{s0}) are plotted vs. time (arbitrary time units). (a) The curves correspond to various values of the *mean-energy detachment rate constant*, $\bar{k}_-$, with a fixed value of the *adhesion energy heterogeneity parameter*, $\sigma = 3.0$. (b) The curves correspond to $\sigma = 0.0$ (solid), 2.0 (dashes), and 4.0 (dotted), with $\bar{k}_- = 1.0$ (arbitrary inverse time units) in each case. This plot shows that for $\sigma > 0$, the model predicts a faster detachment rate for early time, and a slower detachment rate for larger time, than that predicted by the two-parameter model.

in faster decay in $c_s(t)$, similar to that predicted by pure exponential decay ($\sigma = 0$). However, as shown in Figure 10b, for $\sigma > 0$, the three-parameter detachment model predicts a larger rate of detachment for small t, and a smaller rate for large t, than that of the exponential decay model. These results agree with the experimental observations, as shown in Figure 3, where the two models were fitted to the data via nonlinear least-squares regression. As shown by the fitted curves in this example, the three-parameter detachment model provided a much closer fit to the experimental data than the two-parameter (exponential decay) detachment model.

As shown by a plot of the residuals in Figure 11, the three-parameter model fit the data better than the two-parameter model for *Staphylococcus aureus* on the three different polyurethanes and under the four surface treatments. The two-parameter detachment model systematically deviated from the data both at early and later times (Figure 11a), whereas the residuals from the three-parameter model were much more uniformly scattered about zero (Figure 11b). A slight increase in the residuals is apparent at larger t for the three-parameter model, suggesting that at longer times the three-parameter model may slightly underpredict the data for $c_s(t)$.

To justify use of the more complex three-parameter model, its superior fit must be general and not only result from the additional degree of freedom provided by the additional parameter. Because the models are "nested," meaning that the two-parameter detachment model is a limiting case ($\sigma \to 0$) of the more general three-parameter model, a likelihood ratio test was used. In this test, the F distribution was compared to the ratio of the *additional mean-square error* from use of the two-parameter model, over the *mean-square error* of the three-parameter model (Bates and Watts, 1988; Seber and Wild, 1989). Based on pooled data from all samples, a p-value less than 10^{-8} was obtained, strongly rejecting the null hypothesis that the two models equivalently reflect the data, even given the additional degree of freedom of the three-parameter model.

To determine whether the slight upward turn in the residuals from zero that was observed at later times in Figure 11b was statistically significant, a goodness-of-fit test was performed similar to that discussed above for the attachment model. Considering all data from the various surface conditions and the various radial positions that correspond to the same time point as replicates, an analysis of the variance yielded a *p-value* of 0.002, which rejected the hypothesis that the data are uniformly scattered about the model for all time points. It is possible that a systematic deviation may result solely from application of nonlinear regression analysis to a finite number of data points and not necessarily the result of a lack of model validity (Bates and Watts, 1988; Seber and Wild, 1989). However, we suspect the discrepancy results from a slight underprediction of the number of remaining bacteria for later times, as is apparent in Figure 11b. It is possible that either the assumption that each cell has a constant probability per unit time of detaching is not strictly valid, or that k_- is not exactly lognormally distributed among the attached cell population. A physical reason for the former is that $\bar{k}_-$ may slowly decrease with t due to strengthening of the adhesion, thus resulting in the observed underprediction of $c_s(t)$ (Sharma et al., 1992; Meinders and Busscher, 1993). Regardless of the source of this deviation, and considering the few parameters and few physical assumptions involved, we believe the fit of the model to the data satisfactory within our primary goal of defining and measuring an objective index that reflects resistance of the cell to detachment.

Finally, an example of the application of the detachment model is shown in Figure 12, where estimated values of $\bar{k}_-$ and σ is plotted vs. S for detachment of *Staphylococcus au-*

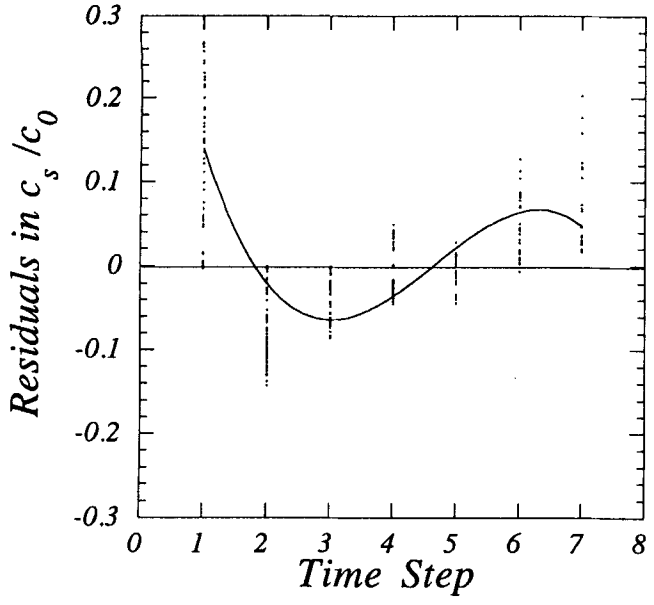

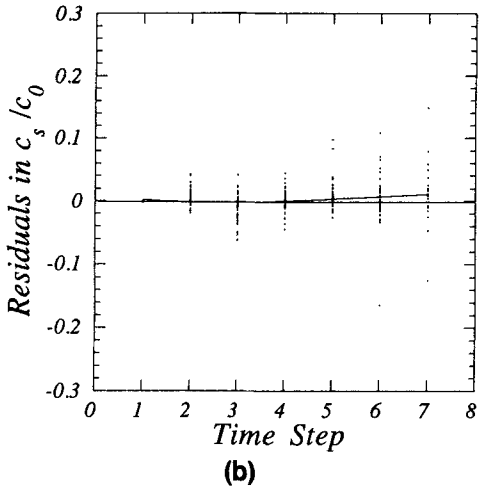

Figure 11. Goodness-of-fit of the detachment model.

The residuals from the nonlinear least-squares regression fit of the model solutions. The experimental data are shown for the detachment of *Staphylococcus aureus* from the three polyurethanes under the four different pretreatment conditions and eight radial positions, using (a) the two-parameter model (equation), and for (b), the three-parameter model. These data suggested a superior fit of the three-parameter model over the two-parameter model, as subsequently confirmed by a statistical analysis of the residuals.

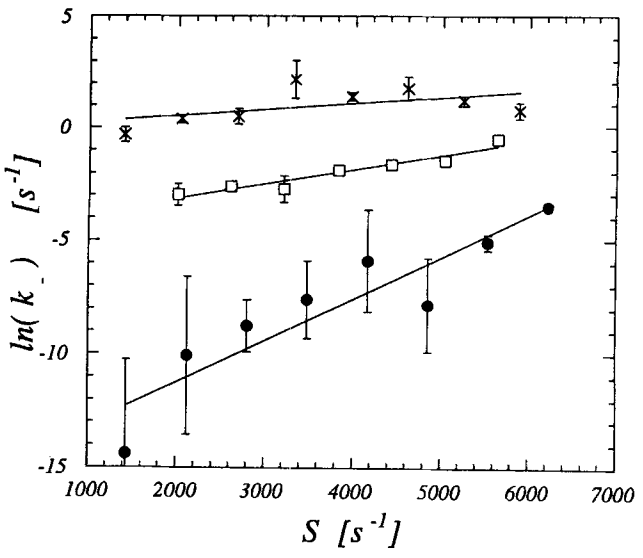

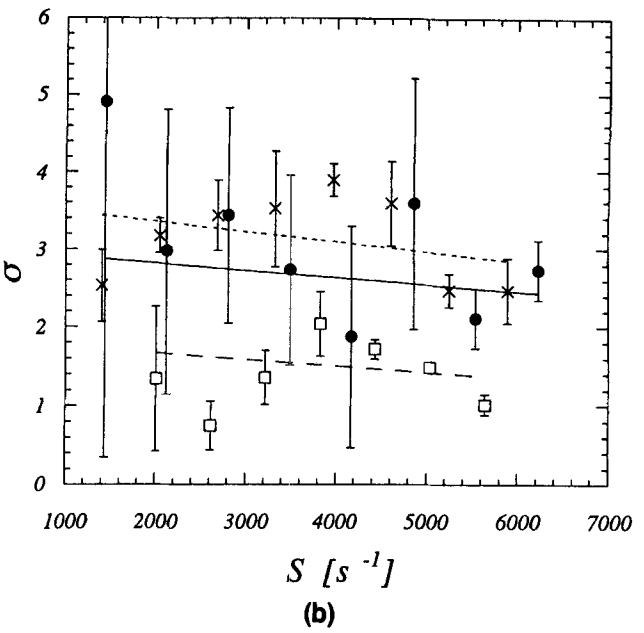

Figure 12. Example of detachment model application.

The regression estimates for (a) the *mean-energy detachment rate constant*, $\bar{k}_-$, and (b) the *adhesion energy heterogeneity coefficient*, σ, are plotted vs. shear rate, S, for detachment of *Staphylococcus aureus* from PEU-S surfaces, pretreated with Fg (circles), HSA (squares), or Bare (crosses).

reus from PEU-S surfaces that were pretreated in three different protein solutions (Fg, HSA, and Bare). In these examples, $\bar{k}_-$ increased approximately exponentially with S, and varied widely with the surface pretreatments. Although there was considerably more scatter in the measurement of σ relative to that of $\bar{k}_-$, σ showed no significant correlation with shear rate, as shown in Figure 12b. This observation is consistent with our hypothesis that σ reflects the heterogeneity in adhesion energy before the initiation of flow.

Discussion

A novel methodology and analysis has been presented to measure intrinsic indices for bacterial attachment and detachment kinetics to biomaterial surfaces as a function of hydrodynamic shear stress. Exploiting the variable shear rate in a radial flow chamber, the attached cell density, $c_s(r, t)$, was measured as a function of radial position, r, and time, t, by recursively acquiring cell counts from multiple fields using an automated videomicroscopy and image analysis system with three-axis motorized stage and focus control. Shear-dependent rate constants for attachment and detachment, k_+ and $\bar{k}_-$, respectively, were then estimated by fitting the solutions of phenomenological models for attachment and detachment kinetics to the experimental data for $c_s(r, t)$. These

parameters are *intrinsic*, in that they reflect only the local interactions between the cell and the surface and local hydrodynamics, not the global transport of cells in the chamber, or other factors that may influence $c_s(r, t)$.

In the attachment experiments, c_s increased linearly with t, suggesting that the rate of detachment was negligible relative to the rate of attachment, and that the presence of attached cells did not influence the attachment of new cells. An *effective attachment rate constant*, k_{eff}, was therefore defined as the rate of increase in c_s divided by the initial cell concentration, c_0. Although k_{eff} provided an overall comparison between attachment rates with different materials or conditions, it did not provide adequate information about the effect of shear on attachment because it depended on the global transport of cells in the chamber (fast attachment leads to a depletion of cells near the surface, and slow attachment leads to an accumulation due to settling). An *intrinsic attachment rate constant*, k_+, that reflects only local interactions between the cell and the surface was therefore defined as the rate of increase in c_s divided by the concentration of cells, $c(r, z)$, near the surface ($z \sim 0$). Using a transport model that predicts $c(r, z)$, k_+ was estimated a function of shear rate, S, by fitting model solutions to the data for k_{eff}. A simply two-parameter exponential relationship for $k_+(S)$ was assumed *a priori*, with a *base attachment rate constant*, k_{+0}, and the *attachment shear-sensitivity coefficient*, δ, as fitted parameters.

The transport model predictions were based on the *surface forces boundary layer approximation*, which assumes that the spatial domain above the chamber surface could be segregated into an "interaction" region and a "bulk" region, and that the flux toward the surface in the interaction region was uniform and proportional to k_+. Hence, k_+ reflects not only the forces and molecular interactions between the cell and the surface, but also the diffusion coefficient and settling velocity within this region (Ruckenstein, 1975; Bowen et al., 1976; Dabros and van de Ven, 1982; Adamczyk et al., 1983; Chari and Rajagopalan, 1985), both of which are expected to be a function of distance from the surface based on the hydrodynamics of an object moving near a surface (Brenner, 1961). Therefore, k_+ depends on the cell's hydrodynamic properties that govern the diffusion coefficient and settling velocity near the surface, in addition to its molecular and physical properties.

Using an experimental methodology similar to that of the attachment experiments, bacterial detachment was also directly observed and quantified in the radial flow chamber. Here, after the bacteria was initially allowed to settle and attach, the flow was initiated to detach the cells. In general, the rate of detachment was found to be extremely slow over the range of shear stresses used in the attachment experiments; therefore, a much higher flow rate was required to induce quantifiable detachment.

An objective intrinsic index was also sought to quantitatively characterize the likelihood of cell detachment from the surface. The simplest assumption was first-order kinetics: the rate of attachment is proportional to c_s with rate constant k_-, which implicitly assumes that the probability (per unit time) of cell detachment was constant with time, and uniform among the attached cell population. The data, however, indicated a faster rate of detachment at earlier time, and a slower rate of detachment at larger times than predicted by first-order kinetics. The hypothesis that the energy of adhesion (and thus k_-) was heterogeneously distributed among the attached cell population was explored by assuming that k_- obeys an Arrhenius-type relationship with the *adhesion energy*, E, and that E was normally distributed among the cell population, resulting in a lognormal distribution for k_-. This assumption led to a three-parameter detachment model (including the initial density, c_{s0}, as a parameter) with a *mean-energy detachment rate constant*, $\bar{k}_-$, and the *adhesion energy heterogeneity coefficient*, σ, to be obtained by a nonlinear least-squares fit of the model to the data. A statistical analysis demonstrated that the superior fit of the three-parameter model was more than expected from the additional degree of freedom alone.

The assumption of a heterogeneous distribution in E is plausible for a homogeneous cell population considering the small dimension and discrete nature of the molecular composition of interface between cell and the surface. Cozens-Roberts et al. (1990a,c) and Saterbak et al. (1993) noted several sources of heterogeneity for the detachment of homogeneous receptor-coated model "cells" in the RFC. These sources included heterogeneity in the size of the contact area, as well as probabilistic variability in the number of bound receptors due to the finite number of receptors and ligands in the contact area.

A probabilistic approach was not necessary to model attachment because all cells in suspension were assumed homogeneous; heterogeneity was only assumed in the possible adhesion state the cell reaches. That is, any cell at a given distance from the surface has equal probability as any other cell at that point of reaching *one of many* possible adhesion states. However, to reverse its course, the attached cell must escape that particular adhesion state it has reached. Therefore, a distribution of available adhesion states creates heterogeneity in the detachment probability, not in the attachment probability.

The behavior of $c_s(t)$ in the phenomenological detachment model presented here is qualitatively similar to that predicted by a mechanistic cell detachment model by Cozens-Roberts et al. (1990a,c) that was based on receptor–ligand binding and dissociation kinetics, when an (approximately) normal distribution for the initial number of bound receptors was assumed (a lognormal distribution with small variance was actually assumed in their model, which is approximately equivalent to a normal distribution). However, in the limit of very small σ, corresponding to a homogeneous cell population with respect to adhesion energy, their model predicted near-deterministic behavior; either all cells detach at nearly the same time, or no cells detach, depending on the strength of fluid shear force. In contrast, the phenomenological model presented here predicts an exponential decay for $c_s(t)$ as σ approaches zero, as predicted by some existing models for detachment of colloid particles from surfaces based on the statistical mechanics of the escape of a particle from a potential well (Dahneke, 1975; Hubbe, 1984). That two models with grossly different predictions for $c_s(t)$ for homogeneous E predict similar behavior for heterogeneous E implies that the characteristic behavior of $c_s(t)$ observed here (fast initial detachment followed by slower detachment at later times) may be relatively robust with respect to the detachment mecha-

nism of an individual cell, but is primarily a manifestation of the assumption that E is approximately normally distributed among the cell population.

Here we examined attachment under a range of shear rates from 35 to 200 s^{-1}. The rate of detachment was found to immeasurably slow over this range; therefore, a higher shear rate range from 1,500 to 7,000 s^{-1} was used to observe detachment. The appropriate shear range of shear rates will depend on the particular application, and can be varied by adjusting the volumetric flow rate. For some surfaces and cell types, both attachment and detachment may be significant under the shear-rate range of interest. In this case, a more complicated model is necessary to simultaneously estimate attachment and detachment rate constants, by including the rate of detachment (cf. Eq. 24) in Eqs. 5 and 7. A similar approach was taken by Meinders et al. (1992, 1994) in a parallel-plate flow chamber, but without obtaining an intrinsic attachment rate constant by solving for the true cell concentration near the surface.

The purpose of the methodology and analysis presented here is not to directly simulate the adhesion events leading pathogenesis in flow configurations found *in vivo*, but rather to provide a direct measurement of the intrinsic probabilities of attachment or detachment as a function of shear rate *in vitro*. This approach could be valuable to both applied and fundamental research on device-centered infections in the effort to provide a rational basis for the design of infection-resistant devices or biomaterials. Because the measured parameters depend only on local interactions and local hydrodynamics, their values should be similar in situations *in vivo* that have similar local hydrodynamics dynamics, limited only by how well the relevant physical properties of the surface, fluid, and bacteria are mimicked *in vitro*. These measurements could aid in device design by allowing prediction of the probability for cell adhesion for a given material and flow configuration. Furthermore, in fundamental studies, measurement of intrinsic parameters allows a direct comparison between the roles of different factors in adhesion, such as the cell's receptor population (Dickinson et al., 1995a), the composition of the adsorbed protein layer (Dickinson et al., 1995a,b), and the surface properties of the biomaterial (Dickinson et al., 1995b). Finally, these comparisons can provide a test for mechanistic theories of bacterial adhesion (Dickinson, 1994).

Acknowledgments

Funding was provided by joint NSF/NIH RFA BCS-91-20660. The authors would like to thank Dr. Richard Proctor and Dorothy Brar, Dept. of Medical Microbiology, University of Wisconsin-Madison, for laboratory and technical assistance with bacterial strains, Dr. Jui-Che Lin, Dept. of Chemical Engineering, University of Wisconsin, for protein purification, Richard Goddard and Dr. James Silver, Dept. of Chemical Engineering, University of Wisconsin, for polymer synthesis. The authors are grateful for assistance and advice from Suzanne Kuo and Dr. Douglas A. Lauffenburger, Dept. of Chemical Engineering, University of Illinois, in the design and application of the radial flow chamber.

Notation

E_1 = activation energy perturbation parameter, erg·s
R = maximum measurable radius in (RFC), cm
u = dimensionless cell concentration
y = dimensionless vertical position
ϵ = dimensionless adhesion energy

Literature Cited

Adamczyk, Z., T. Dapros, J. Czarnecki, and T. G. M. van de Ven, "Particle Transfer to Solid Surfaces," *Adv. Coll. Interf. Sci.*, **19**, 183 (1983).

Bates, D. M., and D. G. Watts, *Nonlinear Regression Analysis and Its Applications*, Wiley, New York (1988).

Bowen, B. D., S. Levine, and N. Epstein, "Fine Particle Deposition in Laminar Flow through Parallel-Plate and Cylindrical Channels," *J. Coll. Interf. Sci.*, **54**(3), 374 (1976).

Brenner, H., "The Slow Motion of a Sphere through a Viscous Fluid Towards a Plane Surface," *Chem. Eng. Sci.*, **16**, 242 (1961).

Bridgett, M. J., M. C. Davies, and S. P. Denyer, "Control of Staphylococcal Adhesion to Polystyrene Surfaces by Polymer Surface Modification with Surfactants," *Biomaterials*, **13**(7), 411 (1992).

Bromberg, J. P., *Physical Chemistry*, Allyn & Bacon, Boston (1984).

Busscher, H. J., G. I. Doornbusch, and H. C. van der Mei, "Adhesion of *Mutans Streptococci* to Glass with and without a Salivary Coating as Studied in a Parallel-Plate Flow Chamber," *J. Dent. Res.*, **71**(3), 491 (1992).

Chari, K., and R. Rajagopalan, "Transport of Colloidal Particles over Energy Barriers," *J. Coll. Interf. Sci.*, **107**(1), 278 (1985).

Cowan, M., and H. J. Busscher, "Flow Chamber Study of the Adhesion of Prevotella Intermedia to Glass after Preconditioning with Mutans Streptococcal Species: Kinetics and Spatial Arrangement," *Microbios*, **73**(295), 135 (1993).

Cozens-Roberts, C., D. A. Lauffenburger, and J. A. Quinn, "Receptor-Mediated Cell Attachment and Detachment Kinetics. I. Probabilistic Model and Analysis," *Biophys. J.*, **58**(4), 841 (1990a).

Cozens-Roberts, C., J. A. Quinn, and D. A. Lauffenburger, "Receptor-Mediated Adhesion Phenomena. Model Studies with the Radial-Flow Detachment Assay," *Biophys. J.*, **58**, 107 (1990b).

Cozens-Roberts, C., J. A. Quinn, and D. A. Lauffenburger, "Receptor-Mediated Cell Attachment and Detachment Kinetics: II. Experimental Model Studies with the Radial-Flow Detachment Assay," *Biophys. J.* **58**(4), 857 (1990c).

Crouch, C. J., H. W. Fowler, and R. E. Spier, "The Adhesion of Animal Cells to Surfaces: The Measurement of Critical Shear Stress Permitting Attachment or Causing Detachment," *J. Chem. Technol. Biotechnol.*, **35B**, 273 (1985).

Cussler, E. L., *Diffusion, Mass Transfer in Fluid Systems*, Cambridge Univ. Press, New York (1984).

Dabros, T., and T. G. M. van de Ven, "Kinetics of Coating by Colloidal Particles," *J. Colloid Interf. Sci.* **89**(1), 232 (1982).

Dahneke, B., "Kinetic Theory of the Escape of Particles from Surfaces," *J. Coll. Interf. Sci.*, **50**(1), 89 (1975).

Dankert, J., A. H. Hogt, and J. Feijen, "Biomedical Polymers: Bacterial Adhesion, Colonization, and Infection," *CRC Crit. Rev. Biocompat.*, **2**, 219 (1986).

Delmi, M., P. Vaudaux, D. P. Lew, and H. Vasey, "Role of Fibronectin in Staphylococcal Adhesion to Metallic Surfaces Used as Models of Orthopaedic Devices," *J. Orthop. Res.*, **12**(3), 432 (1994).

Dickinson, R. B., "A Mechanistic Mathematical Model for Receptor-Mediated Bacterial Adhesion to Biomaterial Surfaces Subjected to Hydrodynamic Shear Stress," AIChE Meeting, San Francisco, paper no. 43h (1994).

Dickinson, R. B., J. A. Nagel, D. McDevitt, T. J. Foster, R. A. Proctor, and S. L. Cooper, "Quantitative Comparison of Clumping Factor- and Coagulase-Mediated Staphylococcus Aureus Adhesion to Surface-Bound Fibrinogen under Flow," *Infect. Immun.*, **63**, 3143 (1995a).

Dickinson, R. B., J. A. Nagel, R. A. Proctor, and S. L. Cooper, "Quantitative Comparison of Shear-Dependent *Staphylococcus aureus* Adhesion to Three Polyurethane Ionomer Analogs with Distinct Fixed Charges," *J. Biomat. Sci. Poly. Ed.*, submitted (1995b).

Dormand, J. R., and P. J. Prince, "A Family of Embedded Runge-Kutta Formulae," *J. Comp. Appl. Math.*, **6**, 19 (1980).

Dougherty, S. H., "Pathobiology of Infection in Prosthetic Devices," *Rev. Infect. Dis.*, **10**, 1102 (1988).

Fowler, H. W., and A. J. McKay, "The Measurement of Microbial Adhesion," *Microbial Adhesion to Surfaces*, R. C. W. Berkeley, J. M. Lynch, J. Melling, P. R. Rutter, and B. Vincent, eds., Ellis Horwood, Chichester, England, p. 143 (1980).

Goddard, R. J., and S. L. Cooper, "Polyurethane Cationomers with Pendant Trialkylammonium Groups: Effects of Ion Content, Alkyl Group, and Neutralizing Anion," *J. Poly. Sci. (B)*, **32**, 1557 (1994).

Goldsmith, H. L., and V. T. Turitto, "Rheological Aspects of Thrombosis and Haemostasis: Basic Principles and Applications," *Thromb. Haemost.*, **55**(3), 415 (1986).

Grasel, T. G., *Surface Properties and Blood Compatibility of Polyurethane Block Copolymers.*, PhD Thesis, Univ. of Wisconsin, Madison (1987).

Grasel, T. G., and S. L. Cooper, "Properties and Biological Interactions of Polyurethane Anionomers: Effect of Sulfonate Incorporation," *J. Biomed. Mater. Res.*, **23**, 311 (1989).

Gristina, A. G., G. Giridhar, B. L. Gabriel, P. T. Naylor, and Q. N. Myrvik, "Cell Biology and Molecular Mechanisms in Artificial Device Infections," *Int. J. Artif. Organs*, **16**(11), 755 (1993).

Gristina, A. G., C. D. Hobgood, and E. Barth, "Biomaterial Specificity, Molecular Mechanisms and Clinical Relevance of *S. epidermidis* and *S. aureus* Infections in Surgery," *Zbl. Bakt. Suppl.*, **16**, 143 (1987).

Hergenrother, R. W., "The Effect of Hard Segment and Ionic Functionality on the Biocompatibility of Polyurethanes," PhD Thesis, Univ. of Wisconsin, Madison (1991).

Herrmann, M., Q. J. Lai, R. M. Albrecht, D. F. Mosher, and R. A. Proctor, "Adhesion of *Staphylococcus Aureus* to Surface-Bound Platelets: Role of Fibrinogen/Fibrin and Platelet Integrins," *J. Infect. Dis.*, **167**, 312 (1993).

Herrmann, M., P. E. Vaudaux, D. Pittet, R. Auckenthaler, P. D. Lew, Schumacher-Perdreau, "Fibronectin, Fibrinogen, and Laminin Act as Mediators of Adherence of Clinical Staphylococcal Isolates to Foreign Material," *J. Infect. Dis.*, **158**, 693 (1988).

Hubbe, M. A., "Theory of Detachment of Colloidal Particles from Flat Surfaces Exposed to Flow," *Colloids Surf.*, **12**, 151 (1984).

Jen, C. J., and J. S. Lin, "Direct Observation of Platelet Adhesion to Fibrinogen- and Fibrin-Coated Surfaces," *Amer. J. Physiol.*, **261**, H1457 (1991).

Lawrence, M. B., C. W. Smith, S. G. Eskin, and L. V. McIntire, "Effect of Venous Shear Stress on CD18-Mediated Neutrophil Adhesion to Cultured Endothelium," *Blood*, **75**(1), 227 (1990).

McDevitt, D., P. Francois, P. Vaudaux, and T. J. Foster, "Molecular Characterization of the Clumping Factor (Fibrinogen Receptor) of *Staphylococcus aureus*," *Mol. Microbiol.*, **11**(2), 237 (1994).

McDevitt, D., P. Vaudaux, and T. J. Foster, "Genetic Evidence that Bound Coagulase of *Staphylococcus aureus* is not Clumping Factor," *Infect. Immun.*, **60**(4), 1514 (1992).

Meinders, J. M., and H. J. Busscher, "Influence of Ionic Strength and Shear Rate on the Desorption of Polystyrene Particles from a Glass Collector as Studied in Parallel-Plate Flow Chamber," *Colloids Surf. A.*, **80**, 279 (1993).

Meinders, J. M., J. Noormans, and H. J. Busscher, "Simultaneous Monitoring of the Adsorption and Desorption of Colloidal Particles During Deposition in a Parallel Plate Flow Chamber," *J. Colloid Interf. Sci.*, **152**(1), 265 (1992).

Meinders, J. M., H. C. van der Mei, and H. J. Busscher, "Physicochemical Aspect of Deposition of *Streptococcus thermophilus B* to Hydrophobic and Hydrophilic Substrata in a Parallel Plate Flow Chamber," *J. Colloid Interf. Sci.*, **164**, 355 (1994).

Moller, P. S., "Radial Flow without Swirl Between Parallel Discs," *Aeronaut. Q.*, **14**, 163 (1963).

Ohtomo, T., and K. Yoshida, "Adhesion of *Staphylococcus aureus* to Fibrinogen, Collagen, and Lectin in Relation to Cell Surface Structure," *Zentralbl. Bakteriol. Mikrobiol. Hyg. [A]*, **268**, 325 (1988).

Paulsson, M., M. Kober, L. C. Freij, M. Stollenwerk, B. Wesslen, and A. Ljungh, "Adhesion of Staphylococci to Chemically Modified and Native Polymers, and the Influence of Preadsorbed Fibronectin, Vitronectin and Fibrinogen," *Biomaterials*, **14**(11), 845 (1993).

Report, N., "Numerical Simulation of Flow Through an Artificial Heart," National Aeronautics and Space Administration, Ames Research Center, (1989).

Ruckenstein, E., "Dynamics of Cell Deposition on Surfaces," *J. Theor. Biol.*, **51**, 429 (1975).

Saterbak, A., S. C. Kuo, and D. A. Lauffenburger, "Heterogeneity and Probabilistic Binding Contributions to Receptor-Mediated Cell Detachment Kinetics," *Biophys. J.*, **65**(1), 243 (1993).

Seber, G. A. F., and C. J. Wild, *Nonlinear Regression*, Wiley, New York (1989).

Sharma, M. M., H. C. Chamoun, D. S. H. Sita Rama Sarma, and R. S. Schechter, "Factors Controlling the Hydrodynamic Detachment of Particles from Surfaces," *J. Colloid Interf. Sci.*, **149**(1), 121 (1992).

Sjollema, J., H. J. Busscher, and A. H. Weerkamp, "Deposition of Oral Streptococci and Polystyrene Particles onto Glass in a Parallel Plate Flow Cell," *Biofouling*, **1**, 101 (1988).

Sjollema, J., H. J. Busscher, and A. H. Weerkamp, "Real-Time Enumeration of Adhering Microorganisms in a Parallel Plate Flow Cell Using Automated Image Analysis," *J. Microbiol. Meth.*, **9**, 73 (1989).

van Kooten, T. G., J. M. Schakenraad, H. C. Van der Mei, and H. J. Busscher, "Development and Use of a Parallel-Plate Flow Chamber for Studying Cellular Adhesion to Solid Surfaces," *J. Biomed. Mat. Res.*, **26**, 725 (1992).

Vaudaux, P., H. Yasuda, M. I. Velazco, E. Huggler, I. Ratti, and F. A. Waldvogel, "Role of Host and Bacterial Factors in Modulating Staphylococcal Adhesion to Implanted Polymer Surfaces," *J. Biomat. Appl.*, **5**, 134 (1990).

Vaudaux, P. E., G. Zulien, E. Huggler, and F. A. Waldvogel, "Attachment of *Staphylococcus aureus* to Polymethylmethacrylate Increases its Resistance to Phagocytosis in Foreign Body Infection," *Infect. Immun.*, **50**, 472 (1985).

Wadstrom, T., "Molecular Aspects of Bacterial Adhesion, Colonization, and Development of Infections Associated with Biomaterials," *J. Invest. Surg.*, **2**(4), 353 (1989).

Wilkinson, P. C., J. M. Lackie, J. V. Forrester, and G. A. Dunn, "Chemokinetic Accumulation of Human Neutrophils on Immune Complex-Coated Substrata: Analysis at a Boundary," *J. Cell Biol.*, **99**(5), 1761 (1984).

Manuscript received June 3, 1994, and revision received Oct. 31, 1994.